

Chapter 2. Theory and design of high efficiency AlGaAs/Si tandem solar cells

2-1. Introduction

The radiative energy from the sun is emitted primarily as electromagnetic radiation from the ultraviolet to infrared and radio spectral region (0.2 to $3\mu\text{m}$). The intensity of solar radiation in free space at the average distance of the earth from the sun is defined as the solar constant with a value of 135.3 mW/cm^2 . The atmosphere attenuates the sunlight when it reaches the earth's surface, mainly due to water-vapor absorption in the infrared, ozone absorption in ultraviolet, and scattering by airborne dust and aerosols. The degree to which the atmosphere affects the sunlight received at the earth's surface is defined by the "air mass". The secant of the angle between the sun and zenith ($\sec\theta$) is called the air mass and the atmosphere path length related to the minimum path length when the sun is directly overhead.

Air mass 1.5 condition (sun at 48.2° above the horizon) represents a satisfactory energy-weighted average for terrestrial applications. The total incident power for AM1.5 is 84.4 mW/cm^2 . In this study, the AM0 is used to evaluate the solar cells, which represents the solar spectrum outside the earth's atmosphere. The AM0 spectrum is the relevant one for satellite and space-vehicle applications, and this spectrum can be also approximated by a 5800K black body radiation. Figure 2-1 shows three curves related to the solar spectral irradiation ¹⁾.

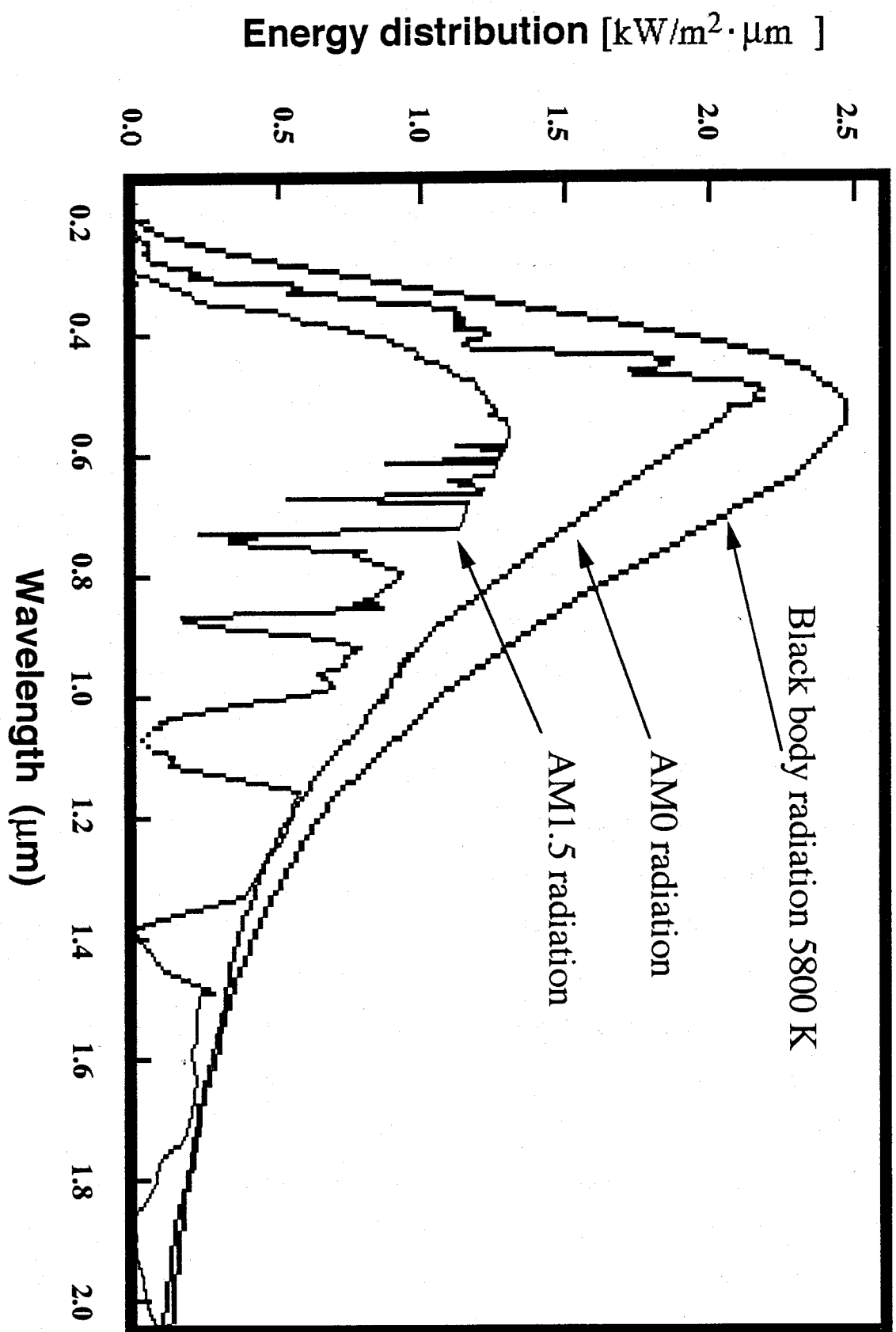


Fig.2-1 Spectral distribution of light outside the earth's atmosphere (AM0), on the surface (AM1.5) and the radiation distribution of a black body at a temperature of 5800K.

A single junction solar cell can convert only a fraction of the incident sunlight into electricity. Such a cell can be designed to be optimally efficient in a limited energy range. Dividing the solar spectrum incident upon an appropriately designed cell would result in great improvement in overall conversion efficiency. The principles of this approach were suggested in 1955 ²⁾. Tandem solar cell has a wider photovoltaic spectral response, which are stacked in tandem with the solar cells of the different energy gaps. In principle, any number of cells can be used in tandem. Method of monolithic connect for tandem solar cell is more convenient to application in comparison with mechanical stack.

In this dissertation, two cells monolithically connected in tandem are involved. The solar cell facing the sun has largest energy gap. This top cell absorbs all the incident photons above its energy gap, and the small energetic photons are transmitted to the cell below. The next cell in the stack absorbs all the transmitted photons with energies equal to or greater than its energy gap. There are three kinds of configurations for two-cell tandem system. In general, two-terminal and three-terminal configuration are usually used in monolithic tandem cells^{3, 4)}, and four-terminal configuration is often employed in mechanical-stack tandem solar cell ^{5, 6)}. Although there is a potential for large increase in conversion efficiency, designing and fabrication of tandem solar cell are more complex than that of a single-junction cell. For example, the top cell must transmit efficiently the photons with less energy than its bandgap. The contacts on the backs of the

upper cell must be transparent to these photons, therefore, cannot be made of usual bulk metal layers. If the cells are connected in series, the thickness and bandgap of individual cell in the stack must be adjusted, so that the photocurrents in all the cells are equal. We prefer to call it as "photocurrent matching condition". For monolithic tandem solar cell, there are effects of growth of the top cell on the characteristics of the bottom cell, and there is the existence of high dislocation density due to the heteroepitaxial growth, which seriously degrades the properties of the top cell. Despite these difficulties, the high efficiency tandem solar cells have been achieved in $\text{Al}_{0.37}\text{Ga}_{0.63}\text{As}/\text{GaAs}$ ⁷⁾ and InGaP/GaAs tandem solar cells⁸⁾. GaAs substrate is expansive and fragile with high-mass-density in comparison with Si substrate. If III-V compounds semiconductor can be successfully grown on Si for solar cell application, it is promising to get high efficiency, large area, low cost tandem solar cells.

In this chapter, the theoretical analyses on $\text{Al}_x\text{Ga}_{1-x}\text{As}/\text{Si}$ ($x=0\sim 0.22$) tandem solar cells are carried out. The device parameters such as the impurity doping concentration, the minority carrier lifetime, the minority carrier diffusion coefficient and the surface recombination velocity are influenced by the device structure and not be independent. The performances of GaAs/Si tandem solar cell in three-terminal configuration and AlGaAs/Si tandem cell in two-terminal configuration are calculated by using device-makeup-dependent parameters determined from experimental observation or from physical judgment based on available information.

Chapter 2-2 Material properties and parameters

2-2-1 Properties and parameters of Si, GaAs and AlGaAs

2-2-1-1 Properties and parameters of Si

2-2-1-1-a) General physical properties of Si

Silicon is the most important material exploited by mankind, and it is the most widely researched and applied semiconductor. Life as we know in the modern world is built around the integrated circuit in our communications, our entertainment, and so on.

Density and lattice parameter of silicon single crystal has been accurately measured. The density is given to be 2.3290028 g/cm^3 at 25°C ⁹⁾. At 1 atm. condition, the lattice constant of Si is $0.543106 \text{ nm}^{10)}$. The room temperature hardness of silicon is usually quoted as being around 1000 kg/mm^2 for all types of indenter profile. The hardness of silicon is found to vary little with temperature up to about 400°C , and the modeling mechanism has been suggested as to be the reversible stress-induced phase transformations¹¹⁾. The thermal expansion coefficient *Alpha* of Si has the relationship with temperature *T* (K) from 120 K to 1500 K, which is proposed as¹²⁾:

$$\text{Alpha} = 3.725 \times 10^{-6} [1 - \exp\{-5.88 \times 10^{-3}(T-124)\}] + 5.548 \times 10^{-10} T (\text{K}^{-1})$$

(2-1)

The thermal conductivity of single crystal silicon exhibits a temperature dependent characteristics of crystal dielectric materials. Representative data from 200 K to the melting point of silicon has been presented¹³⁾. The thermal diffusivity of single crystal silicon is measured in the temperature range 300~1400 K. The data shows that the thermal conductivity continues to decrease with temperature up to almost the melting point¹⁴⁾.

Silicon has an indirect energy gap (E_g) and it is affected by the temperature, pressure and doping concentration. The temperature dependence of $E_g(T)$ was proposed by a semi-empirical formula¹⁵⁾:

$$E_g(T) = E_0 - AT^2 / (T + B) \quad (\text{eV}) \quad (2-2)$$

where E_0 is the energy gap at 0 K, A and B are constants, which are strongly interdependent. $E_0=1.1557$, $A=7.021\times 10^{-4}$, $B=1108$.

The index of refraction (n) and the extinction coefficient (k) are given in the references¹⁶⁻¹⁹⁾. The complex dielectric function N is expressed as $N=n+i\kappa$. The absorption coefficient $\alpha(\lambda)$ can be calculated from extinction coefficient κ , $\alpha=4\pi\kappa/\lambda$, where λ is the wavelength.

2-2-1-1-b) Minority carrier transport properties of Si

(a) p-type Si:

In high purity Si, the measurements²⁰⁻²³⁾ indicate that μ_n is independent of the acceptor concentration (N_A). As the

acceptor concentration increases above $1 \times 10^{16}/\text{cm}^3$, μ_n starts to decrease. Up to the doping level of about $5 \times 10^{17}/\text{cm}^3$, μ_n coincides within the scattering of the available experimental data. A fit to the measured data was given in the reference²⁴⁾:

$$\mu_n = 232 + 1180 / \{1 + [N_A / (8 \times 10^{16})]^{0.9}\} \quad (\text{cm}^2/\text{V} \cdot \text{s}) \quad (2-3)$$

with N_A in cm^{-3} . However, μ_n in the n^+ /p junction increases by as much as four times its bulk value²⁵⁾. The minority-carrier diffusion coefficient (D_n) can be written as:²⁶⁾

$$D_n = 1350 \left(\frac{KT}{q} \right) / \left[1 + 81 N_A / (N_A + 3.2 \times 10^{18}) \right]^{0.5} \quad (\text{cm}^2/\text{s}) \quad (2-4)$$

where K is the Boltzmann constant, T is the absolute temperature and q is the electron charge. In high purity p-type Si, the electron lifetime is also independent of the acceptor concentration but is sensitive to other impurities (O, Fe, or C), the degree of crystal perfection, the cleanliness and thermal history of the fabrication procedures. Beyond an acceptor impurity concentration of about $1 \times 10^{16} \text{ cm}^{-3}$, the electron lifetime begins to decrease as the acceptor density (N_A) increases. The electron lifetime (τ_n) is fitted from the obtained data²⁷⁾:

$$\tau_n = 12 / (1 + N_A / 5.0 \times 10^{16}) \quad (\mu\text{s}) \quad (2-5)$$

The electron diffusion length is the average distance

that an excess electron travels in a field-free p-type semiconductor before recombining. The electron diffusion length L_n can be expressed as $\sqrt{D_n \times \tau_n}$. When $N_A > 10^{18} \text{ cm}^{-3}$, minority-carrier transport parameters reported by Swirhun et al.²⁹⁾ should be used. An approximate fit for doping level over $1 \times 10^{18} \text{ cm}^{-3}$ is²⁸⁾:

$$L_n = 7.13 \times 10^{14} N_A^{(-0.923)} \quad (\text{cm}) \quad (2-6)$$

After processing, L_n is usually much smaller than before processing procedure due to the sensitivity to contaminants and crystal defects.

(b) n-type Si:

In high purity n-type Si, the mobility of minority carrier holes (μ_p) is experimentally found to be independent of donor doping, N_D (cm^{-3}) and the material preparation technique^{28), 30)}. As the donor doping level increases, it starts to decrease. At high doping level, μ_p saturates with doping. The saturation value is, however, about $130 \text{ cm}^2/\text{V}\cdot\text{s}$. A fit to all the available experimental data was given^{31, 32)}:

$$\mu_p = 130 + 370 / \{1 + [N_D / (8 \times 10^{17})]^{1.25}\} \quad (\text{cm}^2/\text{V}\cdot\text{s}) \quad (2-7)$$

The diffusion coefficient (D_p) can be written as:²⁷⁾

$$D_p = 480 (KT/q) / [1 + 350N_p / (N_D + 1.05 \times 10^{19})]^{0.5} \quad (\text{cm}^2/\text{s}) \quad (2-8)$$

In lightly doped n-type silicon, the hole lifetime is

experimentally found to be independent on the donor concentration and very sensitive to the quality of the crystal and cleanliness of the device fabrication process. The highest values of hole lifetime reported in unprocessed n-type Si are of the order of $30 \text{ ms}^{33)}$. As the donor concentration increases beyond about $1 \times 10^{16}/\text{cm}^3$, the hole lifetime is observed to start to decrease. A fit to the available experimental data for donor concentration, N_d , higher than $1 \times 10^{17}/\text{cm}^3$, hole lifetime τ_p was given³¹⁾:

$$1/\tau_p = [(7.8 \times 10^{-13} N_d) + (1.8 \times 10^{-31} N_d^2)] \quad (\text{s}^{-1}) \quad (2-9)$$

However, when the concentration is lower than $1 \times 10^{17}/\text{cm}^3$, the experimental data of the lifetimes varies widely from reference to reference.

As similar as minority carriers in n-type, therefore, the hole diffusion length L_p can be written through following equation: $L_p = \sqrt{D_p \times \tau_p}$. The hole diffusion length L_p decreases very fast as the doping level increases. When the concentration N_d is higher than $1 \times 10^{18} \text{ cm}^{-3}$, the parameters reported by Wang et al.³⁴⁾ should be used. A fit of L_p to the data was given³¹⁾:

$$L_p = 2.77 \times 10^{14} N_d^{-0.941} \quad (\text{cm}) \quad (2-10)$$

(c) Application to solar cells:

The properties of Si material make it very suitable for solar cell application, such as the proper band-gap energy

(1.1eV), the low cost, lower density, large diameter, mechanical strength, high thermal conductivity and abundance of material. Si solar cells began the modern photovoltaic era. Up to today, Si have been highly developed and widely used for solar cells including amorphous Si, poly-Si and crystalline Si in photovoltaic power systems.

2-2-1-2. Properties and parameters of GaAs

2-2-1-2-a) General physical properties of GaAs

GaAs is a fragile material ³⁵⁾. The lattice parameter and density of crystal GaAs were measured accurately by x-ray ³⁶⁾. The respective values are 5.6553 Å and 5.3165 g/cm³. The stiffness constant of GaAs changes quite few with variety of doping concentration. Properties of the variation in the thermal expansion coefficient with temperature ³⁷⁾ are different from that of Si. Above 75 K, the thermal conductivity (C) of GaAs decreases with temperature due to free-carrier scattering, $C = A/T^{1.2}$, where A is a constant which depends on the doping level ³⁸⁾. GaAs has a direct band gap and its absorption coefficient is so large that the incident light can be almost absorbed by only 5 μm-thick GaAs for the wavelength shorter than the energy band gap edge of GaAs. The band gap of GaAs at room temperature is given in the references 39-41). The absorption coefficient of GaAs decreases with increasing temperature ⁴²⁾:

$$E(T) = E_0 - aT^2 / (T + b) \quad (\text{eV}) \quad (2-11)$$

where $E_0 = 1.517$ eV, $a = 5.5 \times 10^{-4}$ (eV·K⁻¹), $b = 225$.

2-2-1-2-b) Minority carrier transport properties of GaAs:

Transport properties of minority carrier in GaAs as a function of temperature, doping level and dislocation density can be considered independently of the growth technique used.

For p-type GaAs, the related datareviews of electron mobility (μ_n) with respect to the doping density are given in the reference ⁴³⁾. The mobility decreases with increase of the doping level. Electron mobility at 300 K ranges from 1150 cm²/V.s for p=3.6×10¹⁸ /cm³ ⁴⁴⁾ to 3500 cm²/V.s at for p=10¹⁷ /cm³ ⁴⁵⁾. Hole diffusion constants (D_p) in n-type GaAs were measured from 7×10¹⁴~1.4×10¹⁸ cm⁻³ ⁴⁶⁾. A rough estimate for D_p is provided by the ref.47):

$$D_p = (KT/q) / [2.5 \times 10^{-3} + 4 \times 10^{-21} N_d] \quad (\text{cm}^2/\text{s}) \quad (2-12)$$

So, the hole mobility can be got from the relationship $D_p/\mu_p = KT/q$.

The minority-carrier lifetime in GaAs is affected by recombination at point defects, surface or interface dislocations, and bulk radiative recombination processes. Nelson et al. carried out systematic study of minority-carrier lifetime in near ideal material ⁴⁸⁾. The measured data shows that the lifetime degenerates rapidly with doping level. Determining the minority-carrier lifetime in GaAs is difficult but important for GaAs solar cells. In general the lifetime is governed by the Shockley-Read-Hall (SRH) recombination, the band-band radiative recombination, and the Auger recombination processes:

$$1/\tau = 1/\tau_{\text{SRH}} + BN + CN^2 \quad (\text{s}^{-1}) \quad (2-13)$$

where τ is the effective minority-carrier lifetime, τ_{SRH} is the

SRH lifetime, B is the coefficient for band-band recombination, C is the coefficient for Auger recombination and N is the doping concentration (N_A or N_D). It has been suggested that τ_{SRH} is of the order of $1\sim 2 \mu s$ and $0.25\sim 0.5 \mu s$ in lightly doped GaAs grown by MOCVD and MBE, respectively ⁴⁹⁾. In practice, however, considerable lifetime deterioration arises during device processing ⁴⁹⁾. Furthermore, as the doping concentration is increased beyond 10^{16} cm^{-3} , τ will decrease in proportional to $1/N^2$ due to the dominance of the Auger recombination.⁵⁰⁾ So, incorporating the above information, the empirical formula can be suggested that for $N \leq 10^{16} \text{ cm}^{-3}$:

$$\tau_n = \tau_p = 0.1 \quad (\mu s) \quad (2-14)$$

For $N > 10^{16} \text{ cm}^{-3}$:

$$\tau = 0.1 / [(N - 10^{16}) / 10^{16}]^{0.5} \quad (\mu s) \quad (2-15)$$

where N is N_A or N_D , τ is τ_n or τ_p , respectively.

GaAs is a very attractive material for solar cells.

- (1) GaAs solar cell has the highest theoretical efficiency limit of about 30% for single junction solar cell under one sun illumination ⁵¹⁾.
- (2) It can be fabricated as thin film cell because 100% optical absorption is achieved in 5 μm -thick GaAs.
- (3) GaAs solar cell shows advantage in severe radiation environments.
- (4) GaAs solar cell shows distinct advantage over silicon at rather high concentration illuminations.

(5) Higher temperature operation than Si solar cell is possible because of its higher bandgap.

However, major disadvantages of GaAs solar cells are expensive, high mass density and fragile compared to silicon solar cells. Combining the advantages of the GaAs and Si material, GaAs/Si technology will provides desired high efficiency, low cost, high performance solar cells to space and terrestrial applications.

2-2-1-3 Properties and parameters of $\text{Al}_x\text{Ga}_{1-x}\text{As}$

General properties and parameters of ternary compounds $\text{Al}_x\text{Ga}_{1-x}\text{As}$ ($0 < x < 1$) vary with alloy composition, x . An interpolation scheme provides a useful tool for estimating some physical parameters of $\text{Al}_x\text{Ga}_{1-x}\text{As}$ compound⁵²⁻⁵⁷⁾. Some material parameters, such as lattice constant, crystal density, thermal expansion coefficient, dielectric constant, and elastic constant obey Vegard's rule well. The linear interpolation of the ternary material parameter $T_{\text{Al},\text{Ga},\text{As}}(x)$ can be written:

$$T_{\text{Al},\text{Ga},\text{As}}(x) = a + bx \quad (2-16)$$

where, a and b are binary parameters (B's) and $a = B_{\text{GaAs}}$, $b = B_{\text{AlAs}} - B_{\text{GaAs}}$. On the other hand, some kinds of material parameters, e.g., electronic-band energy, lattice vibration energy, Debye temperature and impurity ionization energy exhibit quadratic dependence upon composition, x , which can be very efficiently approximated by the relationship:

$$T_{Al_xGa_{1-x}As}(x) = a_1 + b_1x + c_1x^2 \quad (2-17)$$

where, a_1 , b_1 and c_1 are binary parameters, and $a_1=B_{GaAs}$, $b_1=B_{AlAs}-B_{GaAs}+C_{Al-Ga}$, $c_1=-C_{Al-Ga}$. C_{Al-Ga} is a contribution arising from the lattice disorder generated in ternary system $Al_xGa_{1-x}As$. c_1 is called "nonlinear parameter". Some of them are tabulated in Table 2-1 in comparison with GaAs and Si.

Table 2-1 Properties of Si, GaAs and Al_xGa_{1-x}As

properties	Si	GaAs	Al _x Ga _{1-x} As
Lattice constance (Å)	Diamond	Zincblend	Zincblend
Crystal structure	5.431	5.653	$5.6533+0.0078x$
Crystal density (g/cm ³)	2.329	5.360	$5.36-1.6x$
Thermal expansion coefficient ($\times 10^6$ /°C)	2.33	6.4	$6.4-1.2x$
Thermal conductivity (W/cm.K) (300K)	1.5	0.54	$0.44-1.79+2.26x^2$
Electron affinity (eV) (300K)	4.01	4.07	$4.07-1.1x \quad (0 \leq x \leq 0.45)$ $3.64-0.14x \quad (0.45 < x \leq 1)$
Band gap energy (eV) (300K)	1.12	1.42	$1.424+1.247x \quad (0 \leq x \leq 0.45)$ $1.900+0.125x+0.143x^2 \quad (0.45 < x \leq 1)$
Mobility (300K) electron (m ² /V s)	1.12	0.86	
	hole	0.135	0.040
Band Structure	indirect	direct	direct ($x \leq 0.4$) indirect ($x > 0.4$)
mechanical strength	strong	fragile	
Wafer size (inch)	6~8	2~3	
Price	cheap	expensive	

However, minority-carrier transport properties in $\text{Al}_x\text{Ga}_{1-x}\text{As}$ have been hampered to date by a lack of definite knowledge of many basic material parameters. The room temperature electron mobility μ_n in high purity AlGaAs presents three different types of behavior depending on the alloy concentration ⁵⁸⁻⁶⁰⁾:

- (1) The μ_n decreases as the alloy concentration, x , in the direct gap material. The main mechanism limiting the μ_n is the optical phonon scattering and the increase in the electron effective mass.
- (2) In the crossover region, between direct gap and indirect gap material, the transfer of electron to adjacent low mobility minima causes a sharp decrease in the mobility with increasing x . The minimum value of μ_n is attained for $x = 0.45$.
- (3) In the indirect gap region, the mobilities are low and of the order of the pure AlAs mobility.

Data review of μ_n dependent on the Al composition, x , and the carrier concentration at 300 K are carried out by the reference 61). However, the modeling of the scattering mechanisms responsible for the observed hole mobility (μ_p) is very difficult due to the simultaneous presence of two-interacting bands of carriers (light and heavy hole bands) and the nonspherical symmetric nature of the hole wave functions. The dependence of mobility on the carrier-concentration are given by the following empirical formulas:

$$\mu_n = \mu_{n_0} / [1 + (n / n_0)^h] \quad (2-18)$$

$$\mu_p = \mu_{p_0} / [1 + (p / p_0)^j] \quad (2-19)$$

where, $h=0.4$, $n_0=10^{17}/\text{cm}^3$, $j=0.45$, $p_0=6 \times 10^{17}/\text{cm}^3$. n and p are densities of electron and hole, respectively.

The minority-carrier lifetimes in crystalline $\text{Al}_x\text{Ga}_{1-x}\text{As}$ are strongly dependent on the growth technique and the growth conditions. Summary of $\text{Al}_x\text{Ga}_{1-x}\text{As}$ minority-carrier lifetime data with MOCVD method versus aluminum concentration are done in the reference 62).

In general, the deep level concentration is higher than GaAs. It is considered that the higher concentration of other deep states in $\text{Al}_x\text{Ga}_{1-x}\text{As}$ is due to higher activity of aluminum rather than to the fundamental thermodynamic properties of the ternary. The presence of oxygen or water vapor in the growth environment has the effect of dramatically increasing the state concentration in $\text{Al}_x\text{Ga}_{1-x}\text{As}$ in contrast to GaAs, where the effects are negligible⁶³⁾.

There are very few measurements of $\text{Al}_x\text{Ga}_{1-x}\text{As}$ diffusion length in the literature. The diffusion length may be estimated by combining minority-carrier lifetime data with the estimated minority-carrier diffusivity. The latter is usually obtained by extrapolation from the majority-carrier mobility described above and the Einstein relationship. Then the diffusion length is given by square root of the lifetime-diffusivity product.

The minority-carrier lifetime of $\text{Al}_x\text{Ga}_{1-x}\text{As}$ is very structure sensitive. Defects such as deep level impurities, dislocations and surface or interface defects may change

lifetime values by order of magnitude. The measured data ⁶²⁾ indicated similar lifetimes for material grown by either method (MOCVD, LPE, MBE). All data indicate that minority-carrier lifetime decreases dramatically with increase of aluminum content, x . Unlike the case of GaAs, the lifetime does not vary with the inverse of the doping density ⁶⁴⁾. The lifetime has a weak dependence on majority-carrier density ($N_D - N_A$). The lack of doping dependence suggests the Shockley-Read-Hall (SRH) recombination mainly controls the lifetime in $\text{Al}_x\text{Ga}_{1-x}\text{As}$, which can be proved also by the fact that the PL lifetime of $\text{Al}_x\text{Ga}_{1-x}\text{As}$ increases with increasing power of the excited light generally. SRH recombination mechanism is based on minority-carrier capture at near mid-gap energy levels. The deep energy levels are formed by various types of impurities and mechanical defects including surface and interface.

In general, epitaxially-grown $\text{Al}_x\text{Ga}_{1-x}\text{As}$ have been successfully used to application of solar cell, such as, $\text{Al}_x\text{Ga}_{1-x}\text{As}$ top cell for tandem solar cell ^{65,66)}, graded-band-emitter-layer (GBEL)⁶⁷⁾ and window layer for surface passivation of GaAs.

2-2-2 Properties of GaAs grown on Si by MOCVD

The presence of high dislocation density ($10^6 \sim 10^8/cm^2$) and the biaxial tensile stress (about 1kbar at 300K) degrades the crystallinity of GaAs epitaxial layer grown on Si due to the lattice mismatch and the different thermal expansion coefficient between GaAs and Si. The material parameters, especially in minority carrier transport properties have been changed relative to growth on GaAs substrate. It is very important to understand the performance and physical parameters of GaAs heteroepitaxial layer on Si in designing and fabricating the GaAs/Si devices.

1) Surface morphology

A careful choice of Si crystal orientation (usually (100) 2° to 4° degrees off towards [011]), suppresses anti-phase domain and reduces the density of threading dislocations ⁶⁸⁾. Normally, specular surface morphology can be obtained for high quality material. But in fact, the surface of GaAs film grown on Si has an orange peel like texture which can only been in high magnification Nomarski phase contrast images due to deviation from the 3D-like nucleation growth. When GaAs is grown on oxide free Si surface at a substrate temperature about 400°C , the surface always looks very smooth irrespective of the other growth conditions, but the material is optically and electrically inactive. With the two-step growth technique (400°C and 750°C), this problem can be resolved easily. The variation of the thickness is less than $\pm 5\%$.

2) Structure properties

In general, structure properties improve with increasing thickness of GaAs⁶⁹⁻⁷¹⁾. However, when the epitaxial layer is thicker than 4 μm, thin cracks will be caused. During the initial nucleation, RHEED shows a spotty pattern indicating the formation of islands. After a growth of approximately 50 nm thick GaAs, the islands coalescence occurs, the GaAs film is continuous and the RHEED pattern becomes streaky with an excellent 2×4 As-stabilized surface, that indicates high structural quality of the GaAs-on-Si. The Rutherford back scattering spectra (RBS) shows that at 1.5 μm away from the GaAs/Si interface the structural quality of GaAs-on-Si is as good as the bulk GaAs approximately⁷²⁾. As the GaAs thickness increase from 2.1 to 3.5 μm, values of FWHM of double crystal x-ray rocking curves using (400) reflection of GaAs on Si decreases from 290 to 158 arc sec. The FWHM decreases further by post-growth thermal annealing at 850 °C for 5 min⁶⁹⁾.

3) Optical properties:

Optical properties of GaAs-on-Si have been studied by photo luminescence (PL). The biaxial tensile stress shifts the center of gravity of the valence and conduction bands and splits the valence band into $m_j = \pm 3/2$ heavy-hole and $m_j = \pm 1/2$ light-hole subband⁷³⁻⁷⁵⁾. With improved crystal of the GaAs-on-Si film, such as thermal cycle annealing (TCA), the stress in GaAs film increases⁷²⁾. Commensurating with the annealing temperature and the shifts of the emission spectra to longer wavelength are even larger and PL intensity increases with GaAs thickness and thermal annealing^{71), 75)}.

4) Deep level and Defects

The type of defects in GaAs depends on crystal growth technique used. From the study of Schottky diodes and photo-response of avalanche photo-diodes, it has been found that all defects in GaAs-on-Si are not electrically active. Thus GaAs-on-Si with higher crystalline quality and lower defect density may not necessarily have better electrical properties if the defects are more electrically active. Adopting AlGaAs/GaAs superlattices, the dislocation density is reduced to $1 \times 10^6 \text{ cm}^{-2}$ ⁷⁶⁾. Use of InGaAs/GaAs strained layer superlattices and thermal cycle annealing, the dislocation density of 3- μm -thick GaAs on Si is decreased to $3.8 \times 10^6 \text{ cm}^{-2}$ ⁷⁷⁾.

5) Transport properties:

By Hall measurement, in both epitaxial GaAs and modulation doped AlGaAs/GaAs hetero-structure on Si, electron mobilities have been measured which are similar to those on GaAs substrate⁶⁹⁾. But the dislocations degrade minority-carrier transport properties seriously in GaAs-on-Si. The dislocations act as recombination center, so that, minority-carrier devices appear relatively poor performance compared to epitaxial GaAs grown on GaAs substrate. Using $\text{Al}_{0.3}\text{Ga}_{0.7}\text{As}/\text{GaAs}/\text{Al}_{0.3}\text{Ga}_{0.7}\text{As}$ double hetero-structure (DH) with 8 μm -thick GaAs buffer layer, the photo-luminescence lifetime τ_{PL} = 1.75 ns was obtained⁸⁰⁾. Here, $1/\tau_{PL} = 1/\tau_b + 2S/d$, τ_b is the bulk minority-carrier lifetime, S is the interface recombination velocity and d is the active layer thickness. When 10 pairs of $\text{In}_{0.1}\text{Ga}_{0.9}\text{As}/\text{GaAs}$ strained layer superlattice (SLS) was inserted in the GaAs grown on Si and the in-situ thermal cycle

annealing was used, 3 μ m-thick n-type GaAs epitaxial layer has the minority-carrier lifetime of 0.38 ns ⁷⁷⁾.

In summary, the minority-carrier properties of GaAs heteroepitaxial layer on Si is strongly dependent on the growth technique, the device structure, the thickness of the buffer layer, the doping concentration of the active layer, the condition of thermal cycle annealing and so on.

2-3 Design and calculation

2-3-1. Theoretical development

2-3-1-1. Calculated model of $\text{Al}_x\text{Ga}_{1-x}\text{As}$ tandem solar cell

Considerable improvements in Si and GaAs solar cell have been made in the last several years. A crystalline Si solar cell of the efficiency of 23%⁷⁹⁾ and a AlGaAs/GaAs homojunction solar cell of 25.7%⁸⁰⁾ have been demonstrated under one sun AM1.5 condition. Most of the improvement in Si cells has originated from the pyramidal textured surface for light trapping, the front and rear surface passivation to reduce the surface recombination velocity and point-contact for rear electrode. The high efficiency GaAs cells are achieved from the use of InGaP window layer instead of AlGaAs to reduce the surface recombination velocity and the improved GaAs quality using either MBE or MOCVD. J. C. C. Fan et al. proposed two-cell tandem solar cell using GaAs-AlAs/Si or GaAs-GaP/Si systems.⁸¹⁾ Their computer analysis indicates that practical efficiency of about 30% at one sun and over 30% at multiple suns are expected. In other words, GaAs-AlAs/Si system tandem solar cells are very attractive candidates to achieve an inexpensive and efficient solar cell.

This study aims toward providing physical insights into designing the device parameters and optimizing the performance of $\text{Al}_x\text{Ga}_{1-x}\text{As}/\text{Si}$ tandem solar cell. Analyses are concentrated on three-terminal configuration for GaAs/Si tandem solar cell and two-terminal configuration for AlGaAs/Si tandem solar cell, respectively, as the band-gap of $\text{Al}_x\text{Ga}_{1-x}\text{As}$ is changed easily to

meet the photocurrent matching between the top cell and bottom cell. General device physics and equations governing solar cells can be found in refs.82) and 83).

Fig. 2-2. shows a calculated model of GaAs/Si three-terminal tandem solar cell. It consists of a p⁺-n GaAs top cell and a n⁺-p- p⁺ Si bottom cell. The calculation is based on the assumption that the reflection of the solar cell is zero and AlGaAs window layer has no photo-absorption losses. In general, the device parameters like minority-carrier diffusion coefficient and minority-carrier lifetime depend strongly on the material as well as the impurity doping concentration. A successful model describing the minority-carrier lifetime of GaAs-on-Si with relative to the dislocations was proposed by M. Yamaguchi ⁸⁴⁾, and other model indicating effects of the dislocations on the dark-current density of GaAs-on-Si p-n junction was also suggested by John C. Zolper. ⁸⁵⁾

The parameters adopted in the calculation are as follow:
For the Al_xGa_{1-x}As (x=0~0.22) top cell, the front and back interface recombination velocity (S_f and S_{gb}):

$$S_f = 10^4 \quad ; \quad S_{gb} = 10^6 \quad (\text{cm/s}) \quad (2-20)$$

The minority-carrier diffusion coefficients (D_n and D_p) were used as the expressions:⁴⁷⁾

$$D_n = 200 \quad (\text{cm}^2/\text{s}) \quad (2-21)$$

$$D_p = (KT/q)(2.5 \times 10^{-3} + 4 \times 10^{-21} N_D) \quad (\text{cm}^2/\text{s}) \quad (2-22)$$

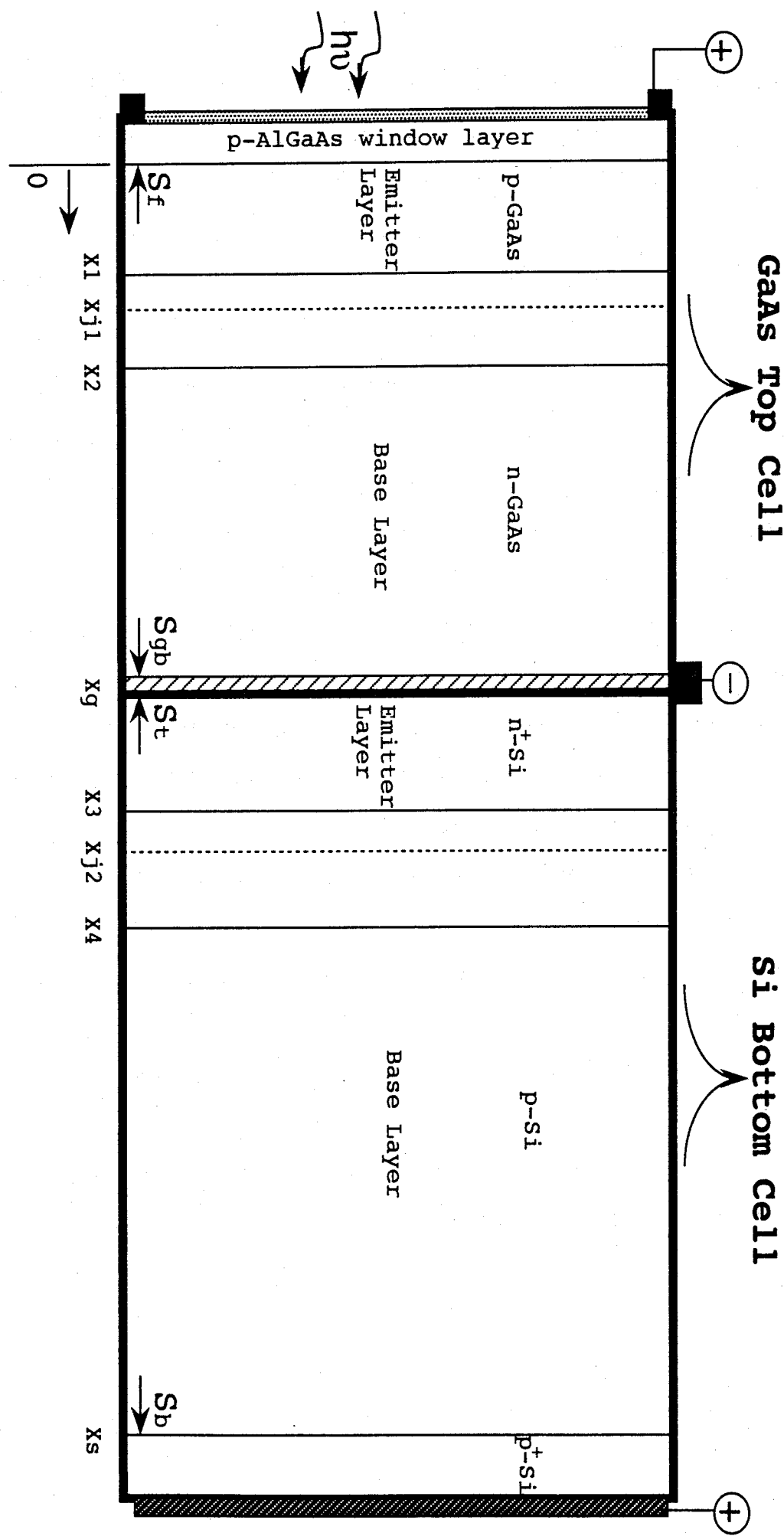


Fig.2-2 The structure of GaAs/Si three-terminal tandem solar cell used in the calculation.

The minority-carrier diffusion length is expressed as ⁸⁶⁾

$$1/L_n^2 = 1/(10 \times 10^{-4})^2 + 1 \times 10^{-12} p + \pi^3 N_d / 4 \quad (\text{cm}^{-2}) \quad (2-23)$$

$$1/L_p^2 = 1/(6 \times 10^{-4})^2 + 1 \times 10^{-11} n + \pi^3 N_d / 4 \quad (\text{cm}^{-2}) \quad (2-24)$$

Where N_d is the dislocation density in GaAs-on-Si. For the Si bottom cell, the parameters described in Chapter 2-2-1-1-b) were used for the calculation. It should be pointed out that the difference of the empirical expressions between nondegraded materials and degraded material (when Si is doped beyond 10^{18} cm^{-3}). The back surface recombination velocity for the Si bottom cell can be approximated as: ⁸⁷⁾

$$S_b = 500 \log N' - 7500 \quad (\text{cm/s}) \quad (2-25)$$

where N' is the base surface doping concentration. For the front surface recombination velocity (S_t), $S_t = 10^2 \text{ (cm/s)}$ is assumed in the calculation.

Fig.2-3 shows the calculated model of the AlGaAs/Si two-terminal tandem solar cell. It consists of a p^+ -n AlGaAs top cell and a p^+ -n-n $^+$ Si bottom cell. In this calculation, we assume that AlGaAs-on-Si material quality is good as AlGaAs-on-GaAs. The minority-carrier parameters of GaAs were used as that of AlGaAs,⁸⁸⁾ but the empirical expressions fitted from the experimental data were used in the calculation. Other parameters and the assumptions were similar to that of the GaAs/Si three-terminal tandem cell.

Al_xGa_{1-x}As Top Cell

Si Bottom Cell

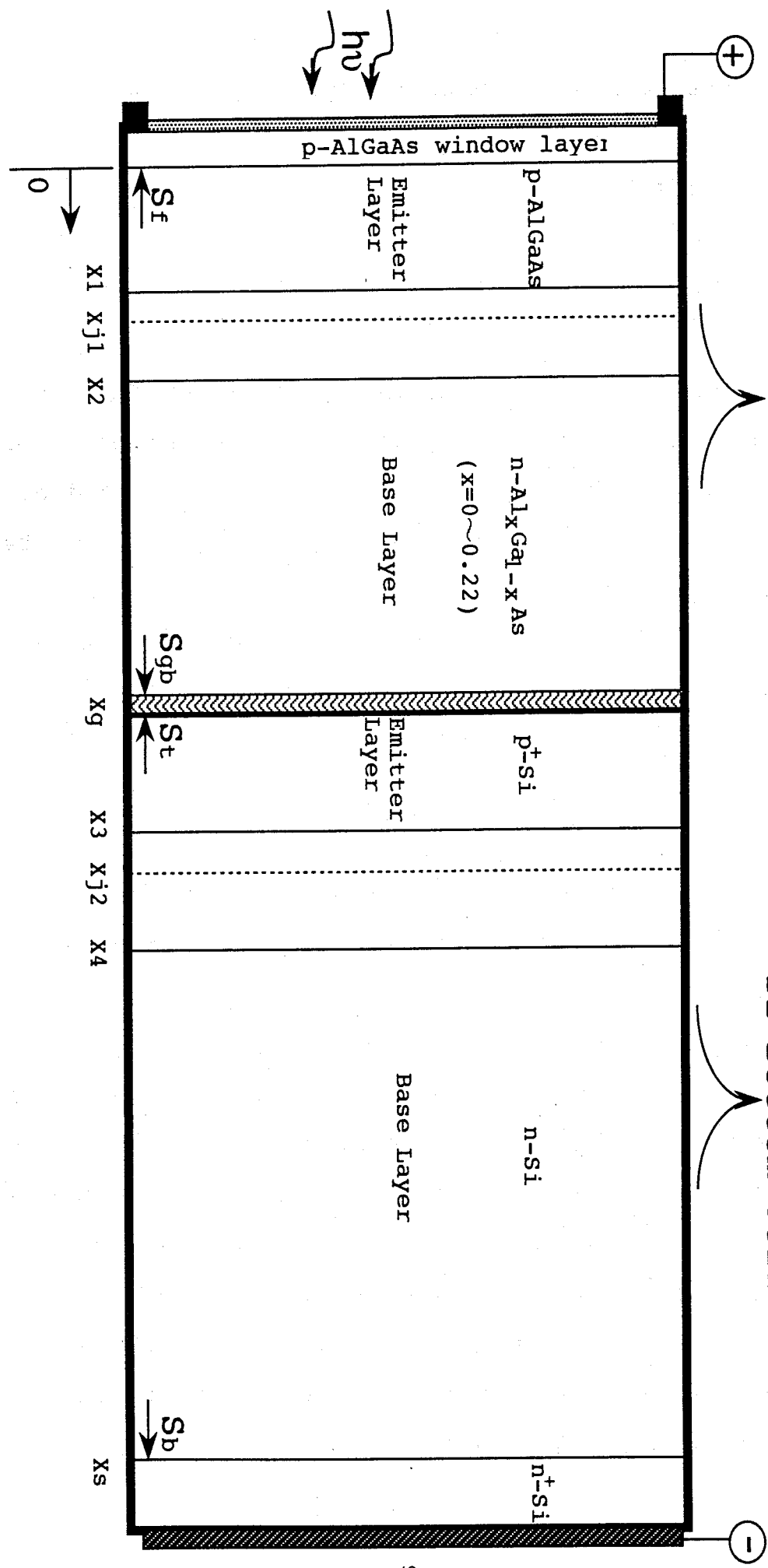


Fig.2-3 The structure of AlGaAs/Si two-terminal tandem solar cell used in the calculation.

Table 2-2. List of symbols

F	photon flux density (AM0)
D _n (D _p)	electron (hole) diffusion coefficient
L _n (L _p)	electron (hole) diffusion length
τ _n (τ _p)	electron (hole) lifetime
n _i	intrinsic free-carrier concentration
N _A (N _D)	acceptor (donor) doping concentration
N _d	dislocation density
K	Boltzmann constant
T	absolute temperature
q	magnitude of electronic charge
α	absorption coefficient
λ	photon wavelength
S _f	front surface recombination velocity of the top cell
S _t	front surface recombination velocity of the bottom cell
S _{gb}	back surface recombination velocity of the top cell
S _b	back surface recombination of the bottom cell
X _{j1} (X _{j2})	junction depth of the top (bottom) cell
J _m	current density at the maximum output
V _m	voltage at the maximum output
J _{p,ph} (J _{n,ph})	photocurrent density collected from p-type (n-type) layer
J _{dr}	photocurrent density collected from the space-charge layer
J _{ph}	total photocurrent density
J _{sc}	short-circuit current density
V _{oc}	open-circuit voltage
FF	fill factor
η	conversion efficiency

2-3-1-2. Formula and equations

1) Short-circuit current density

The photon flux density F (photons $\text{cm}^{-2} \cdot \text{s}^{-1} \text{ nm}^{-1}$) under AM0 condition is used from the measured data.⁸⁹⁾ The total photocurrent density J_{ph} (A/cm^2) at a given wavelength λ collected from the single-junction solar cell is given by

$$J_{ph} = J_{p,ph} + J_{n,ph} + J_{dr} \quad (2-26)$$

The three current densities can be modeled as (considering a uniform p/n junction)⁸²⁾

$$J_{p,ph} = -K_1 \alpha L_n \exp(-\alpha X_1) + \frac{K_1}{(\frac{S_f L_n}{D_n}) \sinh(X_1 / L_n) + \cosh(X_1 / L_n)} \\ \times \{(\frac{S_f L_n}{D_n} + \alpha L_n) - \exp(-\alpha X_1) [(\frac{S_f L_n}{D_n}) \cosh(X_1 / L_n) + \sinh(X_1 / L_n)]\} \quad (2-27)$$

$$J_{n,ph} = K_2 \alpha L_p - \frac{K_2}{(\frac{S_b L_p}{D_p}) \sinh(W_b / L_p) + \cosh(W_b / L_p)} \\ \times \{(\frac{S_b L_p}{D_p}) [\cosh(W_b / L_p) - \exp(-\alpha W_b / L_p)] + \sinh(W_b / L_p) + \alpha L_p \exp(-\alpha W_b)\} \quad (2-28)$$

$$J_{dr} = qF(1-R) \exp(-\alpha X_1) [1 - \exp(-\alpha W)] \quad (2-29)$$

$$K_1 = qF(1-R) \alpha L_n / (\alpha^2 L_n^2 - 1) \quad (2-30)$$

$$K_2 = qF(1-R) \alpha L_p / (\alpha^2 L_p^2 - 1) \exp(-\alpha X_2) \quad (2-31)$$

R is the fraction of photon reflected from the front surface

at given wavelength, $W_b = X_g - X_2$, for the top cell ($W_b = X_s - X_4$ for the bottom cell) and $W = X_2 - X_1$ ($W_b = X_4 - X_3$ for the bottom cell).

When there is constant electric field in the emitter layer, the photocurrent from the emitter region is then:⁸²⁾

$$J_{pp,ph} = -K_{11}[(\alpha + E_{nn})L_{nn} - 1]\exp(-\alpha X_1) + \frac{K_{11}}{(\frac{S_f L_{nn}}{D_n} + E_{nn}L_{nn})\sinh(X_1/L_{nn}) + \cosh(X_1/L_{nn})} \\ \times \{(\alpha + E_{nn})L_{nn}\exp(E_{nn}X_1) - \exp(X_1/L_{nn})\exp(-\alpha X_1) + \\ (\frac{S_f L_{nn}}{D_{nn}} + E_{nn}L_{nn})[\exp(E_{nn}X_1) - \exp(X_1/L_{nn})\exp(-\alpha X_1)]\} \quad (2-32)$$

$$K_{11} = qF(1-R)\alpha L_{nn}/[(\alpha + E_{nn})^2 L_{nn}^2 - 1] \quad (2-33)$$

where E_{nn} is the normalized electric field in the emitter region

$$E_{nn} = qE / 2KT \quad (2-34)$$

and L_{nn} is the effective diffusion length

$$1/L_{nn} = \sqrt{E_{nn}^2 + (1/L_n^2)} \quad (2-35)$$

E is an electric field produced by gradient of the sloped energy edges.

$$E = (-1/q)(\partial E_c / \partial x) \quad (2-36)$$

We assumed that the graded band-gap emitter layer in the GaAs top cell only provides a constant drift field and the varieties of the absorption coefficients were neglected. For

n/p junction cell, all of these equations from (2-26) to (2-34) can be transformed from their present form for p/n cells to equivalents by interchanging L_p , D_p , τ_p and S_p with L_n , D_n , τ_n and S_n , respectively.

The short-circuit current density J_{sc} can be written as

$$J_{scAl_xGa_{1-x}As} = \int_{200(\text{nm})}^{\lambda_G} J_{ph} d\lambda \quad (2-37)$$

$$J_{scSi} = \int_{200(\text{nm})}^{\lambda_Si} J_{ph} d\lambda \quad (2-38)$$

where, $\lambda_G = 1240/E_{gAl_xGa_{1-x}As}$ ($0 \leq x \leq 0.22$) and $\lambda_{Si} = 1240/E_{gSi}$ (nm).

2). open-circuit voltage

In general, when the series resistance R_s of solar cell is neglected, the dark current density J_d in a cell is given by
82)

$$J_d = J_o + J_{dr} \quad (2-39)$$

$$J_o = J_{oo} (\exp[qV/KT] - 1) = (qD_n \frac{n_i^2}{N_A L_n} + qD_p \frac{n_i^2}{N_D L_p}) (\exp[qV/KT] - 1) \quad (2-40)$$

$$J_{dr} = J_{dro} (\exp[qV/2KT] - 1) = qn_i WD / 2L^2 (\exp[qV/2KT] - 1) \quad (2-41)$$

where, D and L are the diffusion coefficient and the diffusion length, J_o is the injection current from p-type and n-type region and J_{dr} is the recombination current in the space-charge

region. For crystal Si solar cells, the injection current density component J_{oo} is assumed to be dominant in the diode saturation current. For the thin-film GaAs cell, the space-charge layer recombination current density component J_{dro} is preferred to be dominant in the saturation component. So, the open-circuit voltage V_{oc} is given by

$$V_{oc} = (KT/q) \ln [J_{sc}/J_{oo} + 1] \quad (2-42)$$

however, for the GaAs cell and the AlGaAs cell

$$V_{oc} = (2KT/q) \ln [J_{sc}/J_{dro} + 1] \quad (2-43)$$

3). Fill factor and conversion efficiency

The output power P (mW/cm^2) of a solar cell is:

$$P = JV = (J_{ph} - J_d)V \quad (2-44)$$

The maximum output power P_m can be derived using $dP/dV=0$

$$P_m = J_m V_m \quad (2-45)$$

where J_m and V_m are the current and voltage at the maximum output point, and V_m can be calculated numerically from the interpolation method easily. The fill factor FF and the conversion efficiency η of the solar cell are defined as

$$FF = J_m V_m / J_{sc} V_{oc} \quad (2-46)$$

$$\eta = P_m / P_{in} \quad (2-47)$$

where $P_{in} = 135.3 \text{mW/cm}^2$ is the incident power at AM0.

For three-terminal configuration, the total conversion efficiency η_{total} of the tandem solar cell is

$$\eta_{total} = (J_{SC_{top}} V_{OC_{top}} F_{F_{top}} + J_{SC_{bottom}} V_{OC_{bottom}} F_{F_{bottom}}) / P_{in} \quad (2-48)$$

For two-terminal configuration, the J_{SC} value used for tandem solar cell is the smaller value of $J_{SC_{top}}$ and $J_{SC_{bottom}}$. For the total conversion efficiency η_{total} of the tandem solar cell is

$$\eta_{total} = J_{SC} F_{F} (V_{OC_{top}} + V_{OC_{bottom}}) / P_{in} \quad (2-49)$$

where J_{SC} and F_F are the short-circuit current and the fill factor of two-terminal tandem solar cell.